



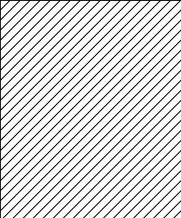
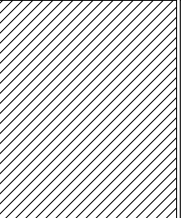
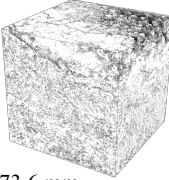
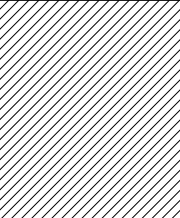
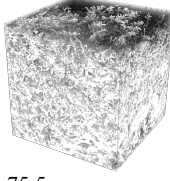
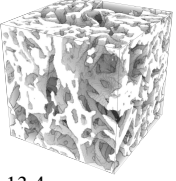
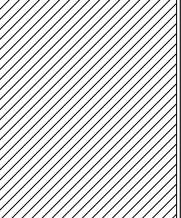
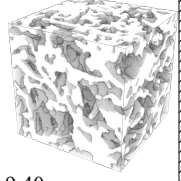
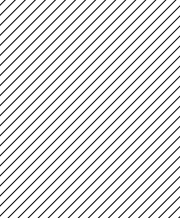
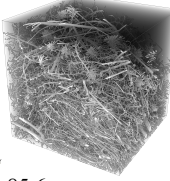
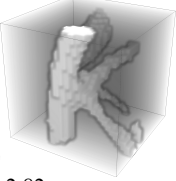
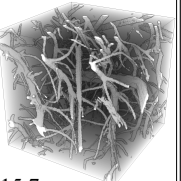
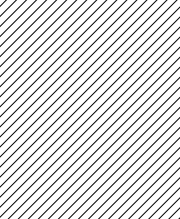
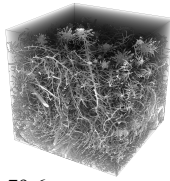
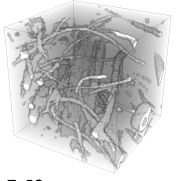
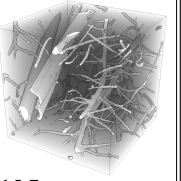
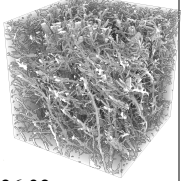
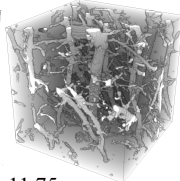
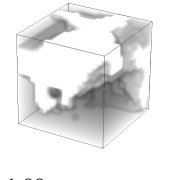
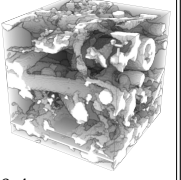
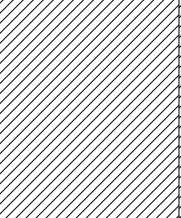
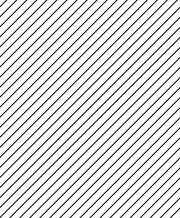
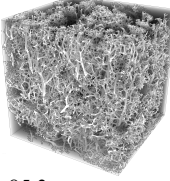
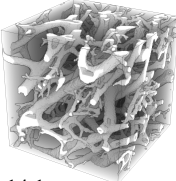
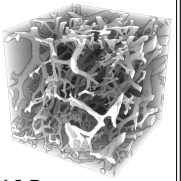
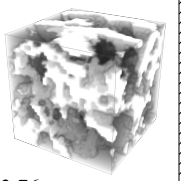
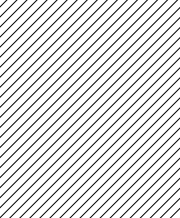
Supplement of

Numerical assessment of morphological and hydraulic properties of moss, lichen and peat from a permafrost peatland

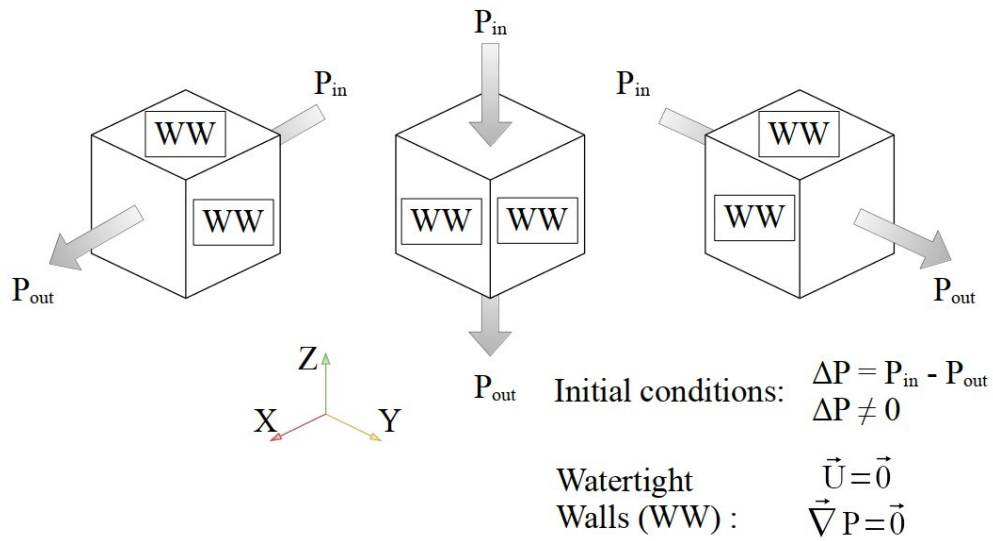
Simon Cazaurang et al.

Correspondence to: Simon Cazaurang (simon.cazaurang@imft.fr)

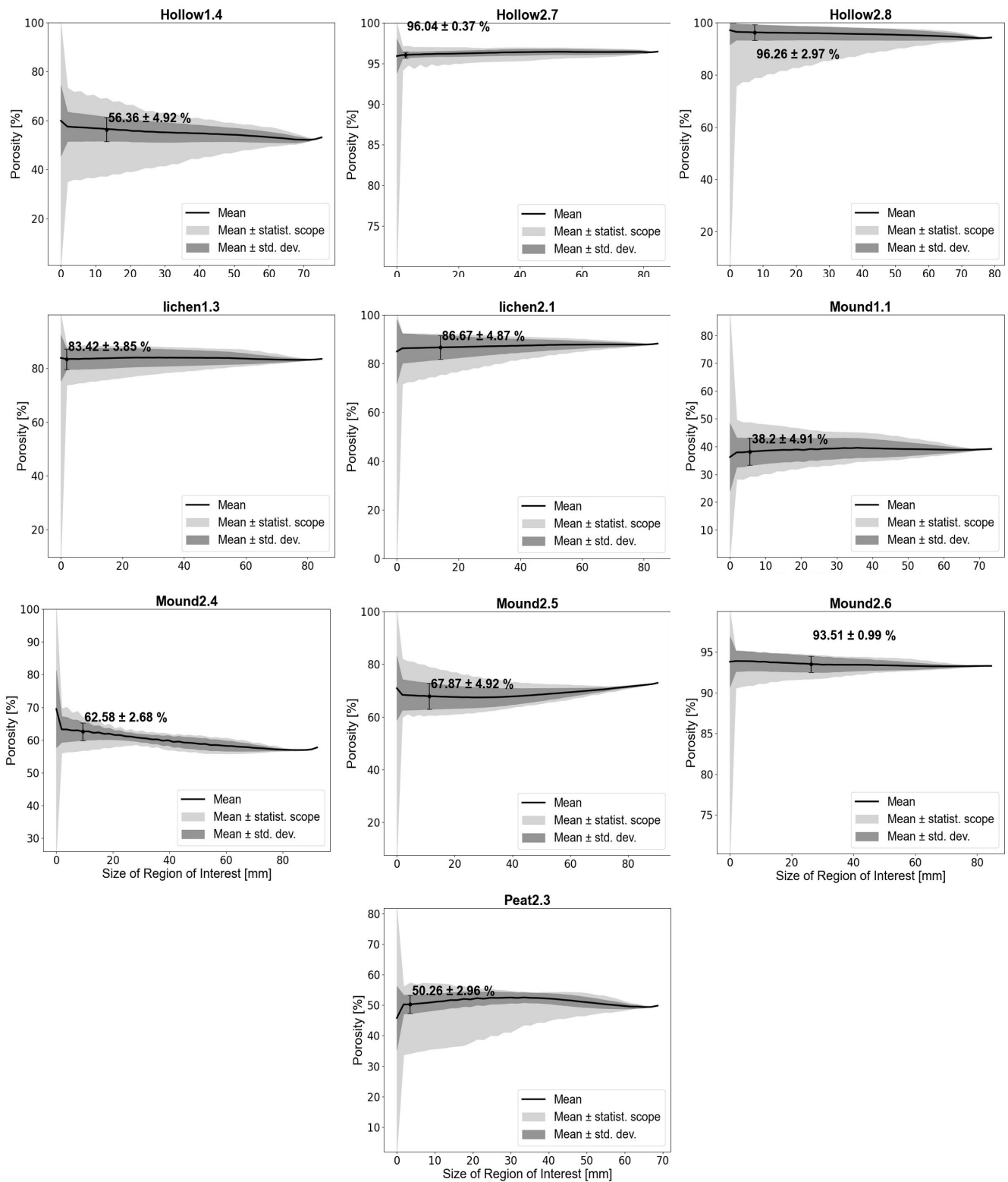
The copyright of individual parts of the supplement might differ from the article licence.

Sample (Specie)	Complete	REV _ε	REV _κ	Sample (Specie)	Complete	REV _ε	REV _κ
Hollow1.2 <i>S. lindbergii</i> Schimp.	 92.6 mm			Mound1.1 <i>S. tenense</i> H. Lindb. ex L.I. Savicz	 73.6 mm	 5.64 mm	
Hollow1.4 <i>S. lindbergii</i> Schimp.	 75.5 mm	 13.4 mm		Mound2.4 <i>S. angustifolium</i> (C.E.O.Jensen ex Russow) C.E.O.Jensen	 93.5 mm	 9.40 mm	
Hollow2.7 <i>S. majus</i> (Russow) C.E.O.Jensen	 85.6 mm	 2.82 mm	 15.7 mm	Mound2.5 <i>S. angustifolium</i> (C.E.O.Jensen ex Russow) C.E.O.Jensen	 90.5 mm	 11.28 mm	
Hollow2.8 <i>S. majus</i> (Russow) C.E.O.Jensen	 79.6 mm	 7.52 mm	 15.7 mm	Mound2.6 <i>S. angustifolium</i> (C.E.O.Jensen ex Russow) C.E.O.Jensen	 86.2 mm	 26.32 mm	 11.75 mm
Lichen1.3 <i>Cladonia. sp.</i>	 85.8 mm	 1.88 mm	 9.4 mm	Peat2.2 -	 79.2 mm		
Lichen2.1 <i>Cladonia. sp.</i>	 85.3 mm	 14.1 mm	 15.7 mm	Peat2.3 -	 75.1 mm	 3.76 mm	

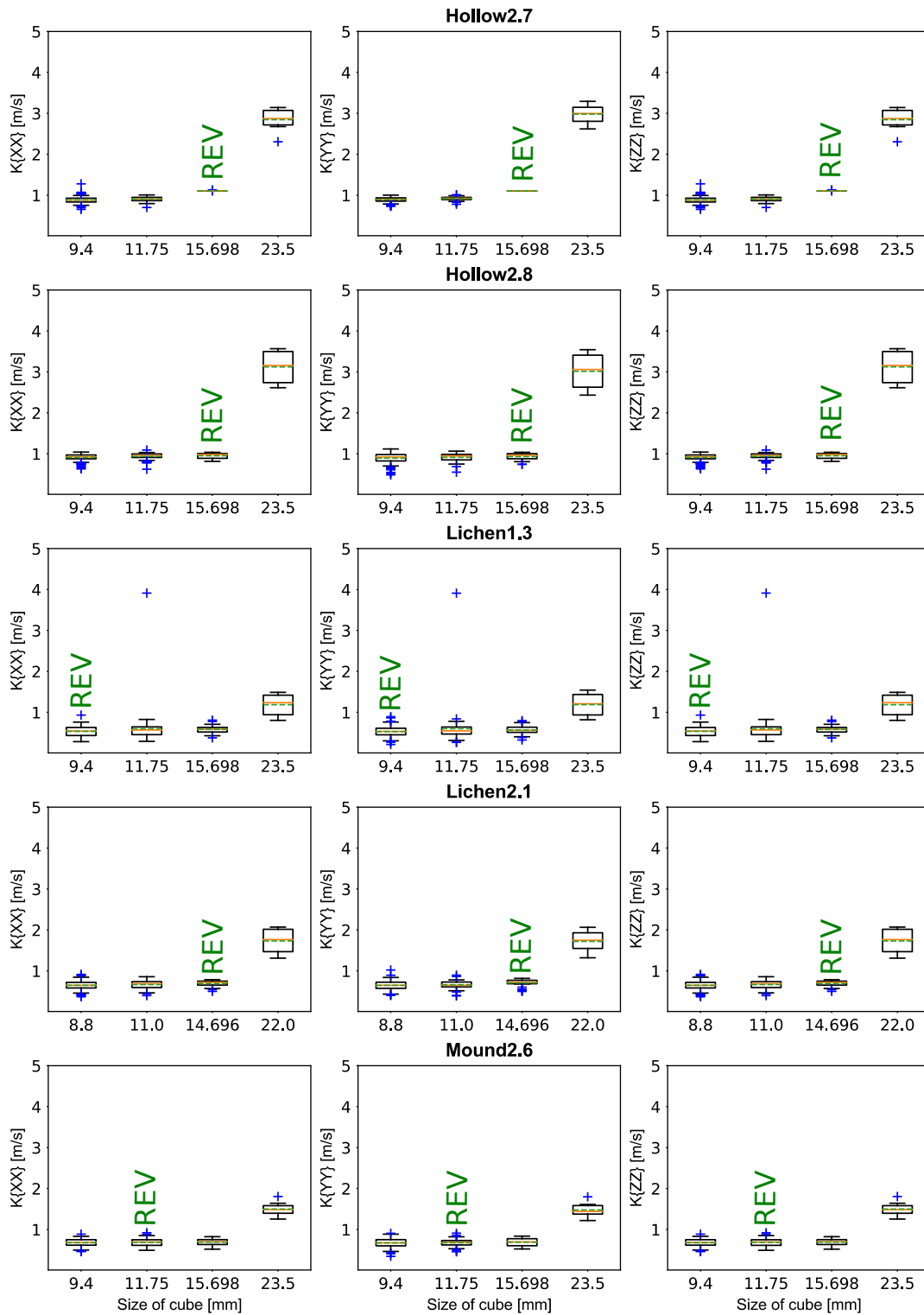
Supplement S1: Global characteristics of collected samples' Usable Volume, numerical reconstructions and examples of Representative Elementary Volumes of Porosity and Hydraulic conductivity. Species were identified according to the morphological descriptions given in Volkova et al. (2018).



Supplement S2: Initial and boundary conditions used for the Direct Numerical Simulation on sub-volumes of samples and pore network models.



Supplement S3: Overview of results of Representative Elementary Volumes of porosity for 10 of 12 samples (2 of them did not converge to a solution). Convergence result for each sample is shown with a point and an error bar.



Supplement S4: Overview of results of Representative Elementary Volumes of hydraulic conductivity for type I samples. Each size matching the minimal standard deviation of diagonal hydraulic conductivity tensor is marked with a “REV” sign.

Supplement S5: Comparison between Direct Numerical Simulations and Pore Network Modeling for homogeneous samples

As a reminder, volume averaging technique requires a sufficient homogeneity on a given property to function properly. In our study, sample of the samples could not be considered as sufficiently homogeneous do to their peculiar structure. Instead, Pore Network Models (PNM) are generated for these samples and properties are then assessed through this proxy.

In this supporting information, a short validation of pore-network against Direct Numerical Simulation is done on homogeneous samples. Then, some details are given on heterogeneous samples' pore network models. This study concludes on clues for choosing either Direct Numerical Simulations or Pore Network Models as a significant and effective property assessment technique.

S5.1. Pore Network validation on morphologically-homogeneous samples

In the main article, we showed that volume averaging methods such as finding a Representative Elementary Volume for each sample is possible if the latter is sufficiently homogeneous upon the given property. For heterogeneous samples, finding a REV does not match the required statistical strength to be considered as a *continuum* of both microscopic and macroscopic. To counterfeit the heterogeneities upon porosity for Type II and Type III samples, we decided to generate a pore network made of interconnected throats and spheres. Then, morphological properties could be then retrieved based on computations directly done on the whole pore network.

To validate this method, the same procedure used for Type II and Type III samples is retroactively applied on Type I samples. Table (S5).1 shows results of a morphological analysis, overall pore network porosity and specific surface area. Then, a ratio is computed to compare respectively porosity and specific surface area obtained from image processing and from pore networks.

Table (S5).1: Morphological properties of Type I based on a pore network model (σ_{S-T} : Ratio between spherical pores and throats; d_{Sph} : Spherical pore density; d_{Thr} : Throat pore density; $\sigma(\epsilon)$: Ratio between image processing-based porosity and pore network-based porosity; $\sigma(S_{SA})$: Ratio between image processing-based specific surface area and pore network-based specific surface area)

Sample	σ_{S-T}	d_{Sph}	d_{Thr}	ϵ^{IP}	ϵ^{PNM}	ϵ^{PNM}	S_{SA}^{IP}	$\sigma(\epsilon)$	$\sigma(S_{SA})$
	[-]	cm^{-3}	cm^{-3}	[%]	[%]	$[m^2 \cdot m^{-3}]$	$[m^2 \cdot m^{-3}]$	[-]	[-]
Lichen1.3 (I)	4.2	$8.3 \cdot 10^1$	$3.5 \cdot 10^2$	83.5	84.9	$7.2 \cdot 10^2$	$2.7 \cdot 10^3$	1.02	3.7
Lichen2.1 (I)	4.4	$7.4 \cdot 10^1$	$3.3 \cdot 10^2$	88.2	89.7	$5.9 \cdot 10^2$	$2.7 \cdot 10^3$	1.04	4.5
Mound2.6 (I)	5.4	$1.2 \cdot 10^2$	$5.9 \cdot 10^2$	93.3	94.5	$3.2 \cdot 10^2$	$3.5 \cdot 10^3$	1.01	$1.09 \cdot 10^1$
Hollow2.7 (I)	5.4	$5.0 \cdot 10^1$	$2.7 \cdot 10^2$	96.5	98.1	$1.6 \cdot 10^2$	$2.5 \cdot 10^3$	1.02	$1.5 \cdot 10^1$
Hollow2.8 (I)	5.2	$5.4 \cdot 10^1$	$2.8 \cdot 10^2$	94.3	96.0	$2.1 \cdot 10^2$	$2.6 \cdot 10^3$	$9.98 \cdot 10^{-1}$	$1.3 \cdot 10^1$

Then, a single-phase flow simulation is made on the whole pore networks in the same way as for Type II and Type III samples. Results for diagonal components of the hydraulic conductivity tensor are available in Table (S5).2.

Table (S5).2: Diagonal components of the hydraulic conductivity tensor (in m.s⁻¹) for the studied type I samples using Pore Network Modeling.

Sample	K_{xx}^{PNM}	K_{yy}^{PNM}	K_{zz}^{PNM}
	[m.s ⁻¹]	[m.s ⁻¹]	[m.s ⁻¹]
Hollow2.7	$4.7 \cdot 10^{-1}$	$4.7 \cdot 10^{-1}$	$3.0 \cdot 10^{-1}$
Hollow2.8	$4.7 \cdot 10^{-1}$	$4.6 \cdot 10^{-1}$	$2.7 \cdot 10^{-1}$
Lichen1.3	$7.7 \cdot 10^{-3}$	$6.9 \cdot 10^{-3}$	$2.7 \cdot 10^{-3}$
Lichen2.1	$3.4 \cdot 10^{-1}$	$3.4 \cdot 10^{-1}$	$2.8 \cdot 10^{-1}$
Mound2.6	$3.4 \cdot 10^{-1}$	$3.4 \cdot 10^{-1}$	$3.0 \cdot 10^{-1}$

To compare hydraulic conductivity results obtained with both methods, a comparative ratio is computed according to the equation given in equation S5.1. Results of these computations are shown in Table (S5).3.

$$\sigma(K_{ii}) = \frac{K_{ii}(PNM)}{K_{ii}(DNS_{REV})} \quad (S5.1)$$

Table (S5).3: Comparison between diagonal components of the hydraulic conductivity tensor (in m.s⁻¹) for the studied type I samples using Direct Numerical Simulation and Pore Network Modeling.

Sample	$\sigma(K_{xx})$	$\sigma(K_{yy})$	$\sigma(K_{zz})$
	[-]	[-]	[-]
Hollow2.7	10^{-2}	10^{-2}	10^{-2}
Hollow2.8	$4.7 \cdot 10^{-1}$	$4.6 \cdot 10^{-1}$	$3.9 \cdot 10^{-1}$
Lichen1.3	$4.9 \cdot 10^{-1}$	$5.0 \cdot 10^{-1}$	$4.2 \cdot 10^{-1}$
Lichen2.1	4.3	4.26	2.8
Mound2.6	$5.0 \cdot 10^{-1}$	$4.9 \cdot 10^{-1}$	$2.9 \cdot 10^{-1}$

A comparison of Pore Size Distribution of Type I samples between image processing and pore network is available in Figure (S5).1.

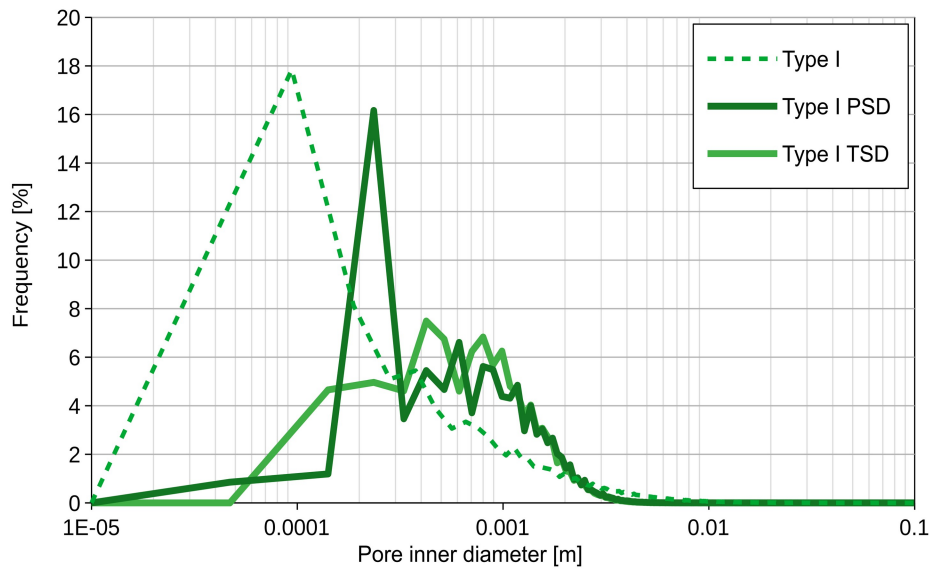


Figure (S5).1: Average Pore Size Distribution (PSD) and Throat Size Distribution (TSD) of Type I sample’s pore networks. The pore size distribution obtained using image processing is shown as a comparison.

PSD and TSD are beginning from smaller sizes and seem more abrupt than pore size distribution obtained by traditional image processing, although median size value is relatively consistent between both methods (between 0.4 and 0.9 mm for the generated pore networks). Most differences appear to be more dependent of PSD and TSD statistical spreads than raw pore sizes. Indeed, pore size distribution computed for Direct Numerical Simulation seems homogeneous if compared to PSD and TSD. Nonetheless, specific surface is always higher using a pore network compared with traditional image processing methods, from one to 15 times higher. This difference could be explained by the fact that the Pore and Throat Size Distributions obtained using Pore Network Modeling have smaller pore diameters than for those obtained using image processing, thus multiplying specific surface.

In terms of morphological properties, comparing Direct Numerical Simulations (DNS) and Pore Network Modeling (PNM) shows that PNM results are in a 5% threshold with DNS results for porosity. However, this is not the case for specific surface area. In this case, PNM results have bigger specific surface areas, up to 15 times higher than results obtained with DNS for Hollow2.7. In terms of hydraulic conductivity, diagonal components are in a one order of magnitude range except for Hollow2.7 sample with PNM results 100 times lower than those found using DNS. This span is still smaller than the observed hydraulic conductivity spread in relation with water saturation (Weber et al., 2017).

It is then possible to conclude that Pore Network Modeling seems to be a valid methodology to bypass heterogeneity problems in porous media.

The case of Hollow2.7 has to be related to the fact this sample is the most porous of the studied sample ($\epsilon > 95\%$). During pore-network generation, image processing artifacts can be mistakenly interpreted causing the split of a throat into many other pores.

S5.2. Morphological description of heterogeneous samples-based pore networks

Parallely to image processing and Direct Numerical Simulations, Pore Network Models (PNMs) are generated from the binarized image stacks. PNMs of type II and III samples are described in detail because they will be used to compute single-phase flow to assess hydraulic conductivity for such heterogeneous samples. Using Direct Numerical Simulations on a complete sample is computationally inefficient and would not lead to sufficient significance. Some information about key morphological values for pore networks of Type II and Type III samples is available in Table (S5).4.

Table (S5).4: Morphological information on Type II and III sample-based Pore Network Models (PNM). σ_{S-T} : Ratio between spherical pores and throats; d_{Sph} : Spherical pore density; d_{Thr} : Throat pore density; S_{SA}^{PNM} : Specific Surface Area calculated on pore network models; $\sigma(S_{SA})$: Comparative ratio between image processing-based specific surface area and pore network-based specific surface area.

Sample	σ_{S-T}	d_{Sph}	d_{Thr}	S_{SA}^{PNM}	$\sigma(S_{SA})$
	[-]	cm^{-3}	cm^{-3}	$[m^2 \cdot m^{-3}]$	[-]
Hollow1.2 (II)	4.2	$7.4 \cdot 10^1$	$3.1 \cdot 10^2$	$2.4 \cdot 10^3$	3.18
Hollow1.4 (II)	3.1	$1.2 \cdot 10^2$	$3.2 \cdot 10^2$	$2.0 \cdot 10^3$	1.58
Peat2.2 (II)	3.6	$7.4 \cdot 10^1$	$2.6 \cdot 10^2$	$2.5 \cdot 10^3$	2.46
Peat2.3 (II)	3.1	$7.8 \cdot 10^1$	$2.4 \cdot 10^2$	$2.3 \cdot 10^3$	1.63
Mound1.1 (III)	2.9	$7.1 \cdot 10^1$	$2.0 \cdot 10^2$	$1.9 \cdot 10^3$	1.20
Mound2.4 (III)	4.1	$1.0 \cdot 10^2$	$4.2 \cdot 10^2$	$2.5 \cdot 10^3$	1.51
Mound2.5 (III)	4.8	$8.6 \cdot 10^1$	$4.1 \cdot 10^2$	$3.0 \cdot 10^3$	2.28

Average Pore Size Distribution (PSD) and Throat Size Distribution (TSD) for Type II and Type III are shown in Fig. (S5).2.

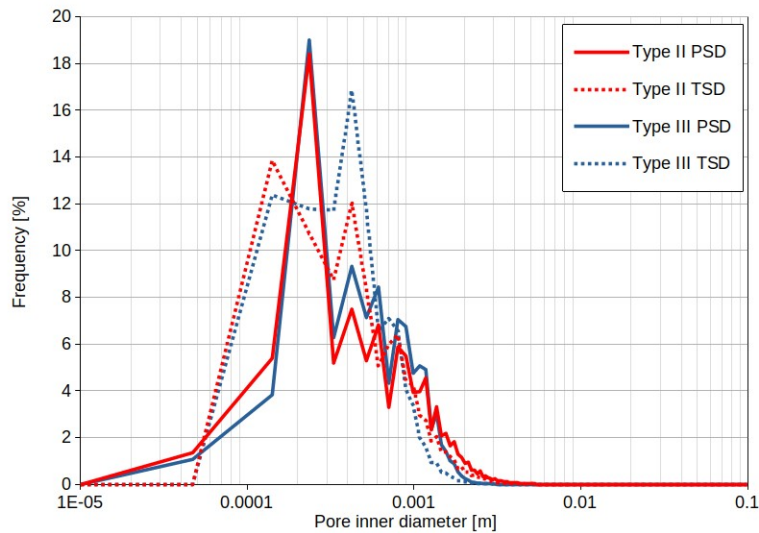


Figure (S5).2: Average Pore Size Distribution (PSD) and Throat Size Distribution (TSD) for Type II and Type III samples based on generated pore network model.

Below this size, Type II shows higher frequencies whereas bigger pores are more frequent for Type III. TSD is closer to a bimodal distribution with a first peak at $1.05 \cdot 10^{-5}$ m and $1.3 \cdot 10^{-5}$ m of pore radii. The first peak is predominant for Type III, the latter for Type II samples. PSD for both Type II and III are equivalent in terms of generic dynamic, with a frequency peak at $1.15 \cdot 10^{-5}$ m of pore radii.

There are from 2.81 to 5.39 times more linking throats than spherical pores. Pore and throat densities fluctuate between 50.1 pores.cm⁻² and 108.8 pores.cm⁻² and between 201.0 throats.cm⁻² and 587.6 throats.cm⁻². These values are independent of sample's nature or classified type, with an overall mean of 4.18 more throats than spherical pores. Therefore, we can assume that spherical pores have mainly four-neighbor connectivity in the generated models. Specific surface area obtained using PNM is always bigger than those obtained by image processing. Biggest deviations are shown by Hollow1.2 and Peat2.2 samples.

S5.3. Direct Numerical Simulations and Pore Network Modeling: which one to choose?

One of the least corresponding sample is Hollow2.7, with specific surface area and hydraulic conductivity being respectively 15 times higher and 100 times lower. One explanation to this could be that high porosity ($\epsilon > 90\%$) is a caveat for pore network generation algorithm. Small artifacts in the base image stack such as isolated pixels could lead to an excessive segmentation of the pore space inducing a smaller pore or throat than reality, thus increasing tortuosity. Some correlations between tortuosity and permeability (and extensively hydraulic conductivity) are assessed in the literature (Koponen et al., 1996). Increasing the tortuosity as well as the connectivity causes the decrease of permeability (and hydraulic conductivity). In the same way, supernumerary throats could also lead to a more fragmented flow path than what is observed in Direct Numerical Simulation.

When porosity is not extreme, PNM seems to enable the reach of effective morphological and hydraulic properties, confirming the possibility to use it on Type II and Type III samples. However, these samples lack of a comparison tool, making the results lower class than those found for Type I samples. Nonetheless, emphasis can be put on the fast processing abilities of PNM to give an efficient estimates of effective properties. Results are obtained in an hour time frame and even less with recent code parallelism upgrades made in *PoreSpy* and *OpenPNM*. In the other hand, DNS requires several days to complete a full hydraulic conductivity study.

Yet, image processing used in this study could lead to an excessive smoothing, eliminating under-resolution pores (not resolvable due to tomograph's own minimal resolution, here 94 μ m) that play an important role in flow dynamics. It would be possible to assume in this case that Direct Numerical Simulation coupled with Representative Elementary Volumes could allow the assessment of phenomena occurring at higher pore sizes, the interplant void space (Baird, 1997). Alternatively, pore network models could be better descriptors for the middle pore size fractions, which corresponds to the space between each *Sphagnum* leaves (intraplant void space, as described by Price & Whittington (2010) and Weber et al. (2017)).